HIGH STRESS INTENSITIES IN FOCUSSING ZONES OF WAVES

J.BALLMANN, H.J.RAATSCHEN and M.STAAT
Lehr- und Forschungsgebiet Mechanik, RWTH Aachen,
Templergraben 64, 5100 Aachen (FRG)

ABSTRACT

The propagation of mechanical waves in plates of isotropic elastic material is investigated. After a short introduction to the understanding of focussing of stress waves in a plate with a curved boundary the method of characteristics is applied to a plate of hyperelastic material. Using this method the propagation of acceleration waves is discussed. Based on this a numerical difference scheme is developed for solving initial-boundary-value problems and applied to two examples: propagation of a point disturbance in a homogeneously finitely strained non-linear elastic plate and geometrical focussing in a linear elastic plate.

INTRODUCTION

Modern investigations on mechanical wave propagation show increasing interest in local stress concentration under transient loading (ref.13).

Experimental investigations of specimens of revolution showed internal cracks due to stress wave focussing (ref.14). The phenomenon of stress concentration caused by focussing can be demonstrated by the ray method in the sequence of figures 1a-c. A plane longitudinal wave travelling along rays is reflected into a longitudinal and a transversal wave due to the free boundary conditions (see Fig. 1a). The envelopes of the reflected rays form two caustics (an incident transversal wave forms a second pair of caustics (see Fig. 1b)), which are the traces of singular points of the wave fronts (see Fig. 1c). Loading plates of transparent materials (PMMA e.g.) in shock tubes the wave fronts can be made visible by shadow photographs (see Fig. 1d and ref.11).

From arguments of geometrical acoustics and from experimental evidence high stresses are expected near the cusps of the caustics. The ray method neglects field effects,however, and gives solutions at the wave front and this only if the solution ahead of the wave is known. But generally this solution is also unknown.

J. Ballmann, H.-J. Raatschen, M. Staat:
High stress intensities in focussing zones of waves.
In P. Ladeveze (Ed.) Local Effects in the Analysis of Structures. Elsevier, Amsterdam (1985) 235-252.
http://opus.bibliothek.fh-aachen.de/opus/volltexte/2009/307/

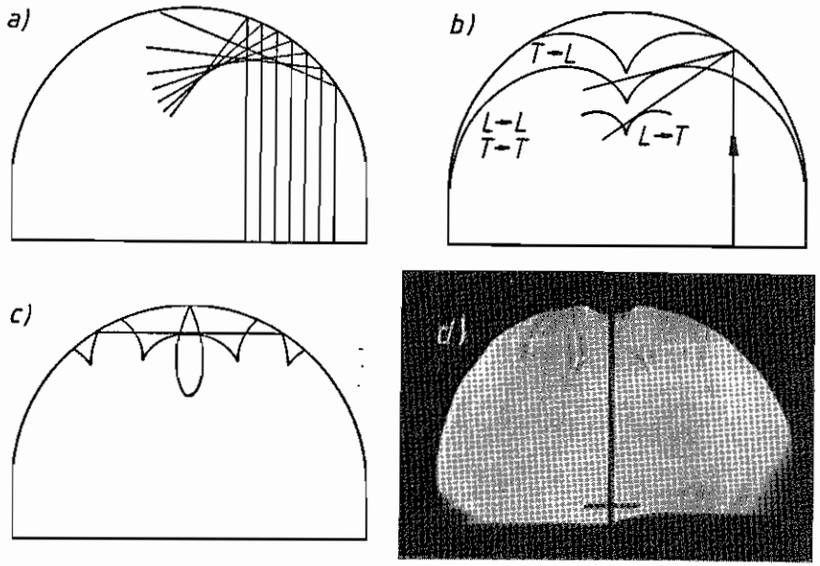

Fig.1. a) Rays of an incident longitudinal wave; b) Caustics; c) Wave fronts at successive times; d) Shadow photograph of the wave fronts (ref.11)

For the numerical solution of elliptical PDEs the application of spatial discretisation procedures especially the finite element method (FEM) is generally accepted. But the great success could not be repeated in the application to hyperbolic PDEs. Even in problems with only one space dimension these methods produce spurious oscillations thus smearing sharp wave fronts (ref.3,17). This is because a local disturbance immediately affects the whole domain of calculation. But physically the wave speed is finite. Moreover, these methods do not treat wave surfaces as discontinuities. Explicit difference schemes e.g. face severe problems with stability because they employ expansions neglecting these discontinuities. Commonly dispersion is controlled by lumping and stability is enforced by using artificial viscosity. A more promising way is the development of finite element methods based on characteristic variables (ref.15).

The method of characteristics was developed for hyperbolic PDEs and became a well established tool for modelling non-linear wave propagation and shock waves in nonsteady gasdynamics (refs.1,10, 12,20). Surfaces that may support discontinuities of some

derivatives of the dependent variables are calculated. By integrating in characteristic surfaces these jumps are not smeared. Explicit difference schemes based on the method of characteristics are stable and reproduce details of the solution with only small dispersion.

Numerical solutions of the complete field equations for the above problem of a semicircular plate were obtained by the authors using the method of characteristics (ref.2).They also applied it to other linear and non-linear problems of elastic plates. Before discussing some results it is felt necessary to explain the method in more detail since it is not yet commonly used in elastodynamics.

The characteristic directions and the so-called compatibility equations for a non-linear elastic plate are derived which are the basis of the numerical scheme. One can find the related equations for linear elastic plates in a similar way or by simplifications of the difference equations.

BASIC EQUATIONS

The position of a material point is given by the Cartesian coordinates x^i and $\bar{x}^i$ (i=1,2,3) in the unstressed reference configuration and in the actual configuration, respectively. Let both sets be connected by a smooth bijective one parameter family of mappings $\bar{x}=\bar{x}(x;\tau)$ with time τ as parameter. The deformation gradient

$$F = \frac{\partial \bar{x}}{\partial x} \qquad (1)$$

is the linear approximation of the mapping. With the displacement $\bar{u} = \bar{x} - x$ the particle velocity $\bar{v}$ and the gradient of displacement are defined as usual (unit tensor 1)

$$\bar{v} = \frac{\partial \bar{u}}{\partial \tau} \qquad (2)$$

$$H = \frac{\partial \bar{u}}{\partial x} = F - 1 \quad . \qquad (3)$$

As strain measures the right CAUCHY-GREEN tensor C and the GREEN strain tensor G are convenient for imcompressible and compressible materials, respectively

$$C = F^T F \qquad (4)$$

$$G = \frac{1}{2} (C - 1) = \frac{1}{2} (H^T + H + H^T H) \quad . \qquad (5)$$

Our discussion is restricted to materials which are hyperelastic, i.e. which have a stored energy density U(C) or U(G). With the symmetric KIRCHHOFF stress σ its variation is

$$\delta U = \frac{1}{2\varrho}\,\sigma : \delta C \quad , \quad \delta U = \frac{1}{\varrho}\,\sigma : \delta G \qquad (6)$$

The mass density ϱ is taken in the reference configuration. The gradient of eq.(6) with respect to the strain measure yields the purely mechanical constitutive equations

$$\sigma_C = \sigma(C) \quad , \quad \sigma_G = \sigma(G) \quad . \qquad (7)$$

The balance of momentum is given by

$$\varrho\,\frac{\partial^2 \bar{u}}{\partial \tau^2} - \operatorname{div}(F\,\sigma) - \varrho\,\bar{k} = 0 \quad .$$

Using eqs.(1)-(7) the balance of momentum can be rewritten into first order PDEs

$$\varrho\,\frac{\partial \bar{v}}{\partial \tau} - \frac{\partial}{\partial F}(F\,\sigma) \vdots \operatorname{grad} H^T + \varrho\,\bar{k} = 0$$

and finally, with the fourth-order elasticities A,

$$\delta F : A : \delta F = \varrho\,\delta^2 U \qquad (8)$$

it reads

$$\varrho\,\frac{\partial \bar{v}}{\partial \tau} - A \vdots \operatorname{grad} H^T + \varrho\,\bar{k} = 0 \quad . \qquad (9)$$

Combining eqs.(2) and (3) yields the integrability equation for $\bar{u}$

$$\frac{\partial H}{\partial \tau} - \operatorname{grad} \bar{v} = 0 \quad . \qquad (10)$$

The material differential operators div and grad are used in the usual manner. Multiple dots denote multiple transvection.

The quasi-linear system of first order PDEs (9),(10) is hyperbolic for the materials under consideration. Therefore certain derivatives of $\bar{v}$ and H may be discontinuous and may propagate as so-called acceleration waves (ref.22). The following discussion is confined to plane stress problems and for compressible materials also to plane strain problems.

THE METHOD OF CHARACTERISTICS

The object of the method of characteristics is twofold. First the characteristic condition determines the directions n^* in which the first order PDEs allow jumps in certain derivatives of the dependent variables. Next these undefined derivatives can be eliminated by forming a linear combination of the original PDEs. The resulting so-called compatibility equation contains only continuous derivatives in a characteristic surface with normal n^*. A star * is used in the text to denote quantities in space and time.

With the independent variables $x^0=c\tau, x^1, x^2$ (c being an arbitrary constant velocity) and the covariant and contravariant base vectors, respectively, e_i and e^j (i,j=0,1,2)

$$e_i\,e^j = \delta_i{}^j \qquad (11)$$

a gradient in space and time is introduced by (α=0,1,2)

$$\nabla^* f = \frac{\partial f}{\partial x^\alpha}\circ e^\alpha \qquad (12)$$

The dyadic product is indicated by the symbol o. Thus the PDEs (9),(10) can be abbreviated (r,s,ϱ,σ=1,...,6)

$$a_r^{*\sigma}\,\nabla^* z_\sigma - c_r = 0 \qquad (13)$$

with unknown functions $z=(\bar{v}^1,\bar{v}^2,H^1{}_1,H^2{}_1,H^1{}_2,H^2{}_2)$, the coefficient matrix of vectors a_r^{*s} and terms c_r containing the unknowns only in a non-differentiated form. The matrix of vectors a_r^{*s} is given by

$$a_r^{*s} = \begin{bmatrix} \varrho c e_0 & 0 & e_1 o \bar{e}^1 o e_1 : A & e_1 o \bar{e}^1 o e_2 : A & e_1 o \bar{e}^2 o e_1 : A & e_1 o \bar{e}^2 o e_2 : A \\ 0 & \varrho c e_0 & e_2 o \bar{e}^1 o e_1 : A & e_2 o \bar{e}^1 o e_2 : A & e_2 o \bar{e}^2 o e_1 : A & e_2 o \bar{e}^2 o e_2 : A \\ -e_1 & 0 & c e_0 & 0 & 0 & 0 \\ 0 & -e_1 & 0 & c e_0 & 0 & 0 \\ -e_2 & 0 & 0 & 0 & c e_0 & 0 \\ 0 & -e_2 & 0 & 0 & 0 & c e_0 \end{bmatrix}$$

The linear combination of eq.(13) with multipliers η^r reads

$$\eta^\varrho\,a_\varrho^{*\sigma}\,\nabla^* z_\sigma - \eta^\varrho\,c_\varrho = 0 \qquad (14)$$

The condition that all remaining derivatives lie in a so-called characteristic surface with normal n^* is equivalent to

$$\eta^r\,a_r^{*s}\,n^* = 0 \qquad (15)$$

This homogeneous system of linear equations has a nontrivial solution η if and only if the coefficient determinant vanishes, i.e. the characteristic equation holds

$$\det(a_r^{*s}\,n^*) = 0. \qquad (16)$$

Choosing the ansatz

$$n^* = -\frac{v}{c}\,e^0 + n \qquad (17)$$

with a space-like unit normal $n = \cos\varphi\,e^1 + \sin\varphi\,e^2$ the characteristic condition eq.(16) becomes a one parameter form for the wave speed v

$$v = v(n) = v(\varphi) \quad .$$

For all the angles $0 \le \varphi < 2\pi$ the vectors n^* generate the normal cone while the corresponding characteristic surfaces envelop the MONGE-cone (see Fig. 2). The generators m^* of the MONGE-cone

$$m^* = c\,e_0 + m \quad , \quad m = \frac{\partial v}{\partial n} \qquad (18)$$

are called bicharacteristics and ensue from the conditions of orthogonality and enveloping

$$\mathfrak{m}^* \, n^* = 0 \quad , \quad \mathfrak{m}^* \, (n^* + \delta n^*) = 0$$

Together with a unit space-like tangent $t = e^o \times n$ the bicharacteristic $\mathfrak{m}^*$ spans the characteristic surface element and so does any near-characteristic $\hat{\mathfrak{m}}$ (ref.21). The possibly natural choice is

$$\hat{\mathfrak{m}}^* = c \, e_o + \hat{\mathfrak{m}} \quad , \quad \hat{\mathfrak{m}} = v \, n$$
$$\hat{\mathfrak{m}}^* = \mathfrak{m}^* - m \, t \quad , \quad \hat{\mathfrak{m}} \, t = 0 \quad . \qquad (19)$$

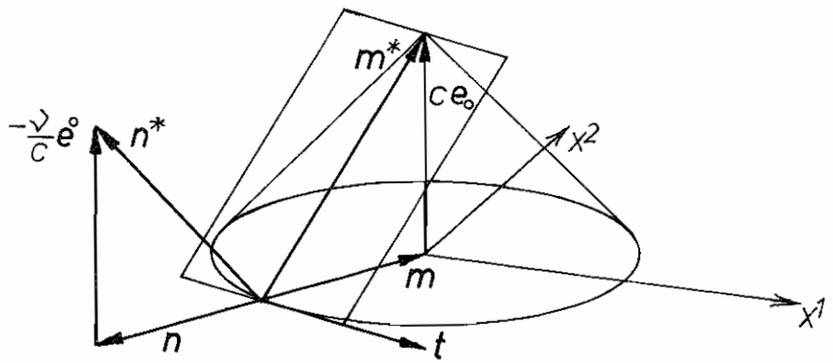

Fig.2. Geometry of characteristic surfaces

Discussion of the Characteristic Condition

After some calculations the characteristic condition reads

$$v^2 \det (\bar{Q}(n) - \varrho v^2 \bar{1}) = 0 \qquad (20)$$

revealing the eigenvalue problem of the acoustic tensor $\bar{Q}$ in the actual configuration

$$\bar{Q} = (\bar{e}_\lambda \circ n : A : \bar{e}^\mu \circ n) \, \bar{e}^\lambda \circ \bar{e}_\mu \qquad (21)$$

The root $v_o = 0$ originates from the special choice of the dependent variables. The related MONGE-cone degenerates to the pathline of a material point. The other roots of the characteristic equation are the eigenvalues of $\bar{Q}$. They can be written with the principal invariants ($I = \mathrm{tr}\bar{Q}$, $II = 0.5(\mathrm{tr}\bar{Q}^2 - I^2)$) leading to

$$\varrho v_\varepsilon^2 = \pm(-0.5 \, I \pm \sqrt{0.25 \, I^2 + II}) \quad , \quad \varepsilon = L, T \qquad (22)$$

Positive and negative roots $v_\varepsilon(n)$ determine the forward and the backward MONGE-cones, respectively. The latter were computed for a highly non-linear material for some state of strain at point P (see Fig.3). For a non-homogeneous deformation these cones are

the local linear approximations of the global MONGE-conoids while the bicharacteristics $\mathfrak{m}^*$ are tangent to their generators which are not plane curves generally.

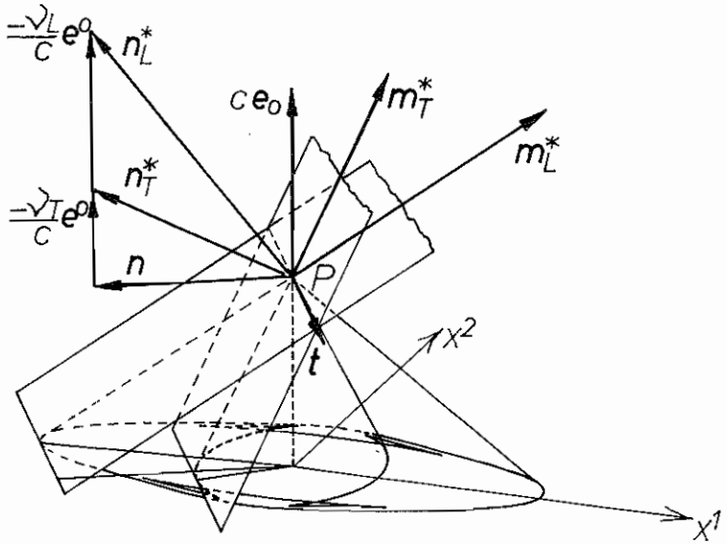

Fig.3. Pathline, quasi-longitudinal and quasi-transversal MONGE-cones

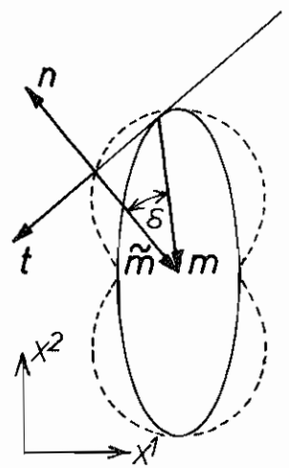

Fig.4. Characteristic loci and FRIEDRICHS diagram

Figure 4 shows a plane intersection of longitudinal MONGE-cones with the plane $c\tau$ = const. together with the solutions of the characteristic condition (20) in broken lines. In gasdynamics these curves are called characteristic loci and FRIEDRICHS diagram, respectively. A plane wave is the trace in space of the characteristic surface. The characteristic loci can either be seen as envelopes of all plane waves that passed through its center P at a time Δt in the past or can be interpreted as the wave fronts in space of a point disturbance at P at the same time (refs.16,18).

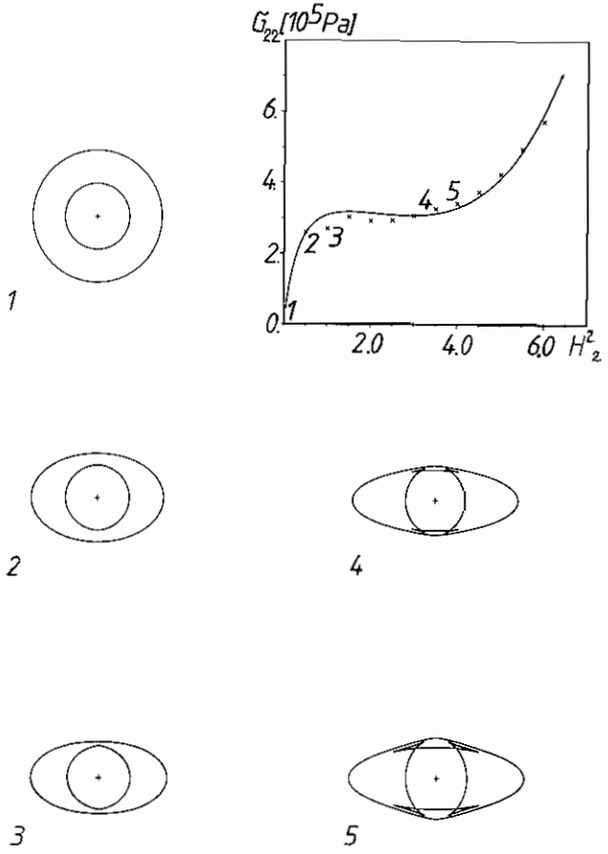

Fig.5. Simple elongation strain path of TRELOAR-material (ref.9 experimental values are denoted by x) and corresponding wave fronts

Plane waves with normal $\mathbf{n}$ travel at their normal speed $\hat{m}_\varepsilon(\mathbf{n})$ while the accompanying discontinuities move along their rays $\mathbf{m}_\varepsilon(\mathbf{n})$ with the angle δ between $\mathbf{m}_\varepsilon$ and the normal direction $\mathbf{n}, \hat{\mathbf{m}}_\varepsilon$. Thus waves are generally quasi-longitudinal and quasi-transversal on the outer and inner MONGE-cone, respectively. For non-linear materials pure modes propagate along the axes of symmetry where $\delta=0$. Since these coincide with the principal axes of $\boldsymbol{\sigma}, \mathbf{C}$ and $\mathbf{G}$ for isotropic materials corresponding waves were termed principal waves (ref.22).

For some isotropic materials the variety of wave fronts is achievable as observed for different linear anisotropic materials (refs.4,16,19). The example in figure 5 shows an incompressible material with simple elongation strain path in direction $\mathbf{e}_2$. The KIRCHHOFF stress σ_{22} was calculated from data given for TRELOAR-material (ref.9). For the numbered deformations the calculated wave fronts are shown. Note that there are either 0,2 or 4 cusped triangles on the quasi-transversal front. It could be proved for linear anisotropic materials that the interior of the wave front cuspoidal triangles are stable lacunae that are gaps in the range of influence where the displacement, associated with an impulsive disturbance at the vertex of the forward MONGE-cone, vanishes identically (refs.5,18). In the linear elastic case the wave fronts emenating from a point are circles as in figure 5 for the undeformed state (N$^{\circ}$ 1).

Compatibility Equations

Eq.(15) provides a set of multipliers η^r_ε $(r=1,\ldots,6)$ for each solution v_ε of the characteristic condition (16),(20). For each set of η^r_ε eq.(15) can be formulated;
along the pathline ($\varepsilon=0$):

$$\nabla^* \mathbf{H} : \mathbf{t} \circ \mathbf{m}^*_\varepsilon = \nabla^* \bar{\mathbf{v}}\, \mathbf{t} \qquad (23)$$

along the cones ($\varepsilon=L,T$):

$$\varrho v_\varepsilon\, \bar{\mathbf{q}}_\varepsilon \circ \mathbf{m}^*_\varepsilon : \nabla^* \bar{\mathbf{v}} - \bar{\mathbf{q}}_\varepsilon \circ \mathbf{n} : \mathbf{A} \circ \mathbf{m}_\varepsilon : \nabla^* \mathbf{H} = r_\varepsilon \qquad (24)$$

with $$r_\varepsilon = \bar{\mathbf{q}}_\varepsilon \circ \mathbf{n} : \mathbf{A}\, \mathbf{t} \circ \mathbf{t} : \nabla^* \bar{\mathbf{v}} - v_\varepsilon\, \bar{\mathbf{q}}_\varepsilon \circ \mathbf{t} : \mathbf{A} \circ \mathbf{t} : \nabla^* \mathbf{H} - \varrho v_\varepsilon \bar{\mathbf{q}}_\varepsilon \bar{\mathbf{k}}$$
$$-\varrho v_\varepsilon (\mathbf{m}_\varepsilon \mathbf{t}) \bar{\mathbf{q}}_\varepsilon \circ \mathbf{t} : \nabla^* \bar{\mathbf{v}} + (\mathbf{m}_\varepsilon \mathbf{t}) \bar{\mathbf{q}}_\varepsilon \circ \mathbf{n} : \mathbf{A} \circ \mathbf{t} : \nabla^* \mathbf{H}$$

Herein $\bar{\mathbf{q}}_\varepsilon$ denotes the normed eigenvector of $\bar{\mathbf{Q}}$.

Eqs.(23),(24) contain only interior derivatives in the direction of $\mathbf{m}^*_\varepsilon$ and $\mathbf{t}$ and lack any outward derivative in the direction of $\mathbf{n}^*$. Hence all derivatives lie on the characteristic surface and eq.(23) cannot lead out of it. As a consequence all

functions and gradients on the characteristic surface are continuous, while they may be discontinuous across it. Eqs. (23),(24) are the so-called compatibility equations. Initial values on characteristic surfaces must be prescribed compatible with them.

Choosing $\hat{\mathbf{m}}^*_\varepsilon$ of eq.(19) instead of $\mathbf{m}^*_\varepsilon$ may be advantageous to simplify eq.(24). Note, there is no difference between $\hat{\mathbf{m}}^*_\varepsilon$ and $\mathbf{m}^*_\varepsilon$ on principal axes.

$$\varrho v_\varepsilon \, \bar{q}_\varepsilon \circ \hat{\mathbf{m}}^*_\varepsilon : \nabla^* \bar{v} - \bar{q}_\varepsilon \circ \mathbf{n} : \mathbf{A} \circ \hat{\mathbf{m}}^*_\varepsilon : \nabla^* H = \mathfrak{F}_\varepsilon \qquad (25)$$

$$\mathfrak{F}_\varepsilon = \bar{q}_\varepsilon \circ \mathbf{n} : \mathbf{A} \; \mathbf{t} \circ \mathbf{t} : \nabla^* \bar{v} - v_\varepsilon \bar{q}_\varepsilon \circ \mathbf{t} : \mathbf{A} \circ \mathbf{t} : \nabla^* H - \varrho v_\varepsilon \bar{q}_\varepsilon \bar{k} \quad .$$

A difference scheme for the numerical solution of elastic problems is developed from the physically reasoned eqs.(18),(23),(24) or (19),(23),(25) in the next section.

DIFFERENCE EQUATIONS

Given the initial data on the surface $\tau = t_o$ a solution at point P on the surface $\tau = t_o + \Delta t$ is obtained numerically by integrating the compatibility equations along characteristics passing through P. Having done this for all points of the solution surface $\tau = t_o + \Delta t$ it is used as new initial surface, and the process repeated until the complete range of influence specified by the initial data has been determined.

For convenience introduce a differential operator on characteristic ε ($\varepsilon = 0, L, T$)

$$\frac{Dy}{D\tau}\Big|_\varepsilon = \nabla^* y \; \mathbf{m}^*_\varepsilon \qquad (26)$$

with y to be integrated. Time τ is used as parameter of integration. Integrating eq.(26) gives

$$y(t_o+\Delta t) - y(t_o) = \int_{to}^{t_o+\Delta t} (\nabla^* y \; \mathbf{m}^*_\varepsilon) \, D\tau$$

and with a TAYLOR-expansion of the integrand

$$y(t_o+\Delta t) - y(t_o) = 0.5\left((\nabla^* y \; \mathbf{m}^*_\varepsilon)\Big|_{t_o+\Delta t} + (\nabla^* y \; \hat{\mathbf{m}}^*_\varepsilon)\Big|_{t_o}\right)\Delta t + o(\Delta t^3) \qquad (27)$$

Here $(\nabla^* y \; \hat{\mathbf{m}}^*_\varepsilon)|_{to}$ is preferred rather than $(\nabla^* y \; \mathbf{m}^*_\varepsilon)|_{to}$ to maintain the space-like normal n along the path of integration. The domain of dependence of $P(t_o+\Delta t)$ is found by applying eq.(27) to the position vector, $y = x$

$$x(t_o+\Delta t) - x(t_o) = 0.5 \left(\mathbf{m}_\varepsilon\Big|_{t_o+\Delta t} + \hat{\mathbf{m}}_\varepsilon\Big|_{t_o}\right) \Delta t + o(\Delta t^3) \; . \qquad (28)$$

Note, $\mathbf{m}_\varepsilon$ and $\hat{\mathbf{m}}_\varepsilon$ depend on the solution at P; $\varepsilon = L, T$.

Integration of the compatibility equations leads to the following difference equations along the pathline:

$$H\Big|_{t_o+\Delta t} - H\Big|_{t_o} = 0.5\left(((\nabla^* \bar{v})\,1)\Big|_{t_o+\Delta t} + ((\nabla^* \bar{v})\,1)\Big|_{t_o}\right)\Delta t + o(\Delta t^3) \qquad (29)$$

along the cones:

$$\begin{aligned} &\left(\left(\varrho v_\varepsilon \, \bar{q}_\varepsilon\right)\Big|_{t_o+\Delta t} + \left(\varrho v_\varepsilon \, \bar{q}_\varepsilon\right)\Big|_{t_o}\right)\left(\bar{v}\Big|_{t_o+\Delta t} - \bar{v}\Big|_{t_o}\right) - \\ &-\left((\bar{q}_\varepsilon \circ \mathbf{n}:\mathbf{A})\Big|_{t_o+\Delta t} + (\bar{q}_\varepsilon \circ \mathbf{n}:\mathbf{A})\Big|_{t_o}\right):\left(H\Big|_{t_o+\Delta t} - H\Big|_{t_o}\right) = \qquad (30) \\ &= \left(r_\varepsilon\Big|_{t_o+\Delta t} + \mathfrak{F}_\varepsilon\Big|_{t_o}\right)\Delta t + o(\Delta t^3) \end{aligned}$$

The TAYLOR-expansion of the coefficients and the right side of eqs.(29),(30) is admissible because all quantities are continuous as long as no shocks occur and have continuous first derivatives in the characteristic surface.

Difference equations (30) may be formulated along any characteristic. They employ the values of the six unknown functions and their space-like inner derivatives. Choosing the eigenvectors of σ at point P as a basis for a local scheme four of the eighteen unknowns become decoupled. Four equations are formulated along the pathline and both cones, respectively. The balance of momentum integrated along the pathline is used to complete the system by two (non-characteristic) equations (refs.6,7). The space-like inner derivatives are eliminated explicitely, leaving a set of six non-linear algebraic equations for the solution at P which is solved iteratively for the non-linear case. For an initial guess $\bar{v}$ is not needed because it is not employed in the constitutive law eq.(6) and thus does not enter the coefficients in eq.(30). Hence it is sufficient to integrate the compatibility equations along the pathline

$$H\Big|_{t_o+\Delta t} - H\Big|_{t_o} = ((\nabla^* \bar{v})\,1)\Big|_{t_o} \Delta t + o(\Delta t^2) \; . \qquad (31)$$

A suitable net is employed for the spatial discretisation. Then the required values and their derivatives on the initial surface are calculated from the local approximation by a second order surface in a least squares sence. The COURANT-FRIEDRICHS-LEWY stability condition (ref.8) is satisfied if the analytical domain of dependence is a subset of the numerical domain of dependence as represented by the points employed in the approximation. Numerical dispersion is reduced by choosing points that are close to the

outer cone. Unfortunately the stability condition is but necessary and is sufficient for linear systems of PDEs only. In figure 6 some typical numerical schemes as used for the calculation are shown for inner points and for points on boundaries.

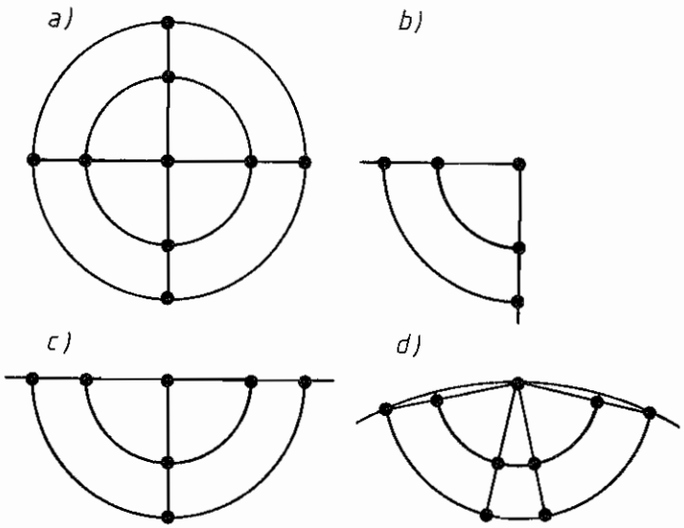

Fig.6 Numerical schemes: a) inner point, b) corner point, c) point on straight boundary, d) point on curved boundary

EXAMPLES

Point Disturbance in a Nonlinear-Elastic Plate

For testing the properties of the numerical scheme a point disturbance in an homogeneously deformed plate is investigated. The material of figure 5 in state N^o 5 was used for the example, with the higher principal strain C_{22} so that the faster principal longitudinal wave propagates in direction e_2. At time $\tau=0$ an initial disturbance $\bar{v}^2$ is introduced at the centre of the plate. It propagates along the quasi-transversal MONGE-conoid (see fig. 7a). The perspective view and the contour lines clearly show the influence of the lacunae (see fig. 5). The components $H^2{}_1$ and $H^2{}_2$ move also along the inner cone whereas $\bar{v}^1$ (see fig. 7b), $H^1{}_2$ and $H^1{}_1$ propagate along the quasi-longitudinal MONGE-conoid predominantly.

Apparently the numerical scheme maintains the structure of the local wave fronts in the global field. There is no sign of any precursors of the fronts.

Geometrical Focussing in a Linear Elastic Plate

The local stress concentration due to geometrical focussing is calculated for a rectangular, linear elastic plate with one semicircular boundary. The front side (opposite the curved boundary) is subjected to constant stress σ_{22} while all other boundaries are free of stresses. The incident longitudinal wave undergoes a phase shift when reflected at the boundary. Tensile stresses increase when the wave front approaches the geometrical focus. From geometrical accoustics we expect the highest stresses at the cusps of the caustics. The cusp of the caustic of the reflected longitudinal wave is located on the axis of symmetry at 0.5 of the radius.

The sequences in figures 8a,b show the principal stresses σ_I and σ_{II}. The first picture is taken when the whole domain is disturbed. In the following time steps the maximum values move towards the focus and increase. The highest values are reached in the third picture in the assumed area. Then the wave amplitudes decrease.

CONCLUSIONS

The numerical method of bicharacteristics is appropiate to the computation of transient wave motion. Also for the non-linear problem it models the physically anisotropic propagation of waves correctly. The described difference scheme can be applied also to waves in linear transversely isotropic elastic plates. The method proved suitable for strong discontinuities with focussing effects. Furthermore shocks can be included in the numerical scheme as sharp discontinuities as is well-known in gasdynamics.

ACKNOWLEDGEMENTS

We are indebted to the Deutsche Forschungsgemeinschaft which partly supported our work through the SFB 27. We are grateful to Prof. H. Grönig and A. Henckels of the Stoßwellenlabor, Aachen for supplying the shadow photograph.

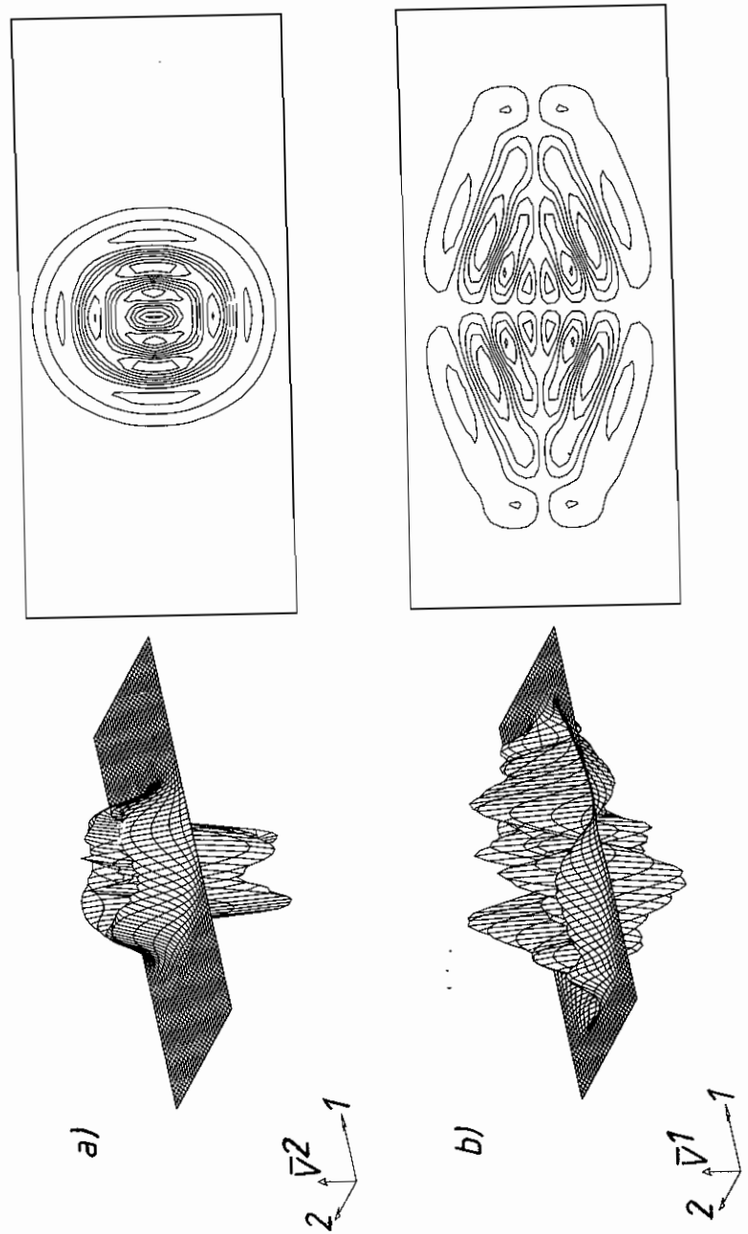

Fig.7. Perspective view and contour lines for a point disturbance in a non-linear elastic plate
a) velocity $\bar{v}^2$, b) velocity $\bar{v}^1$

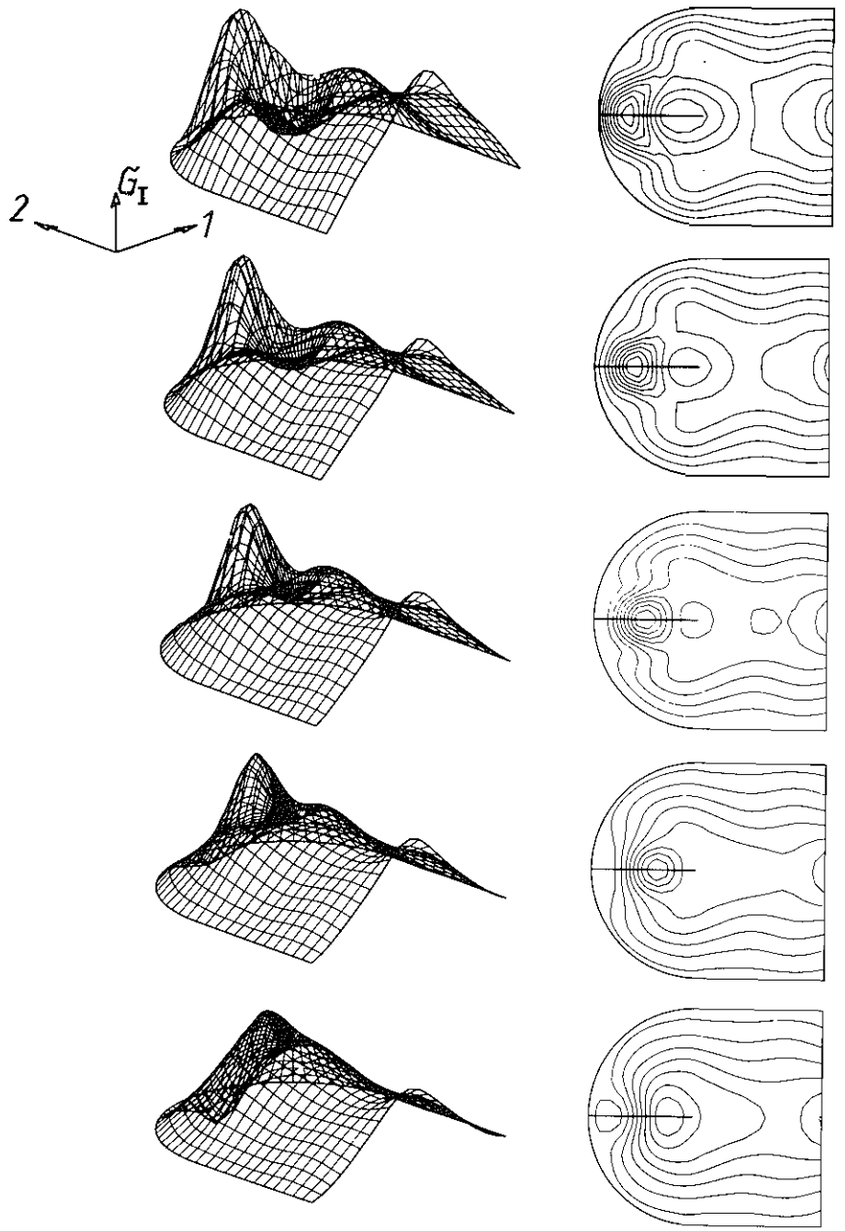

Fig.8a Perspective view and contour lines of principal stress σ_I for successive time steps

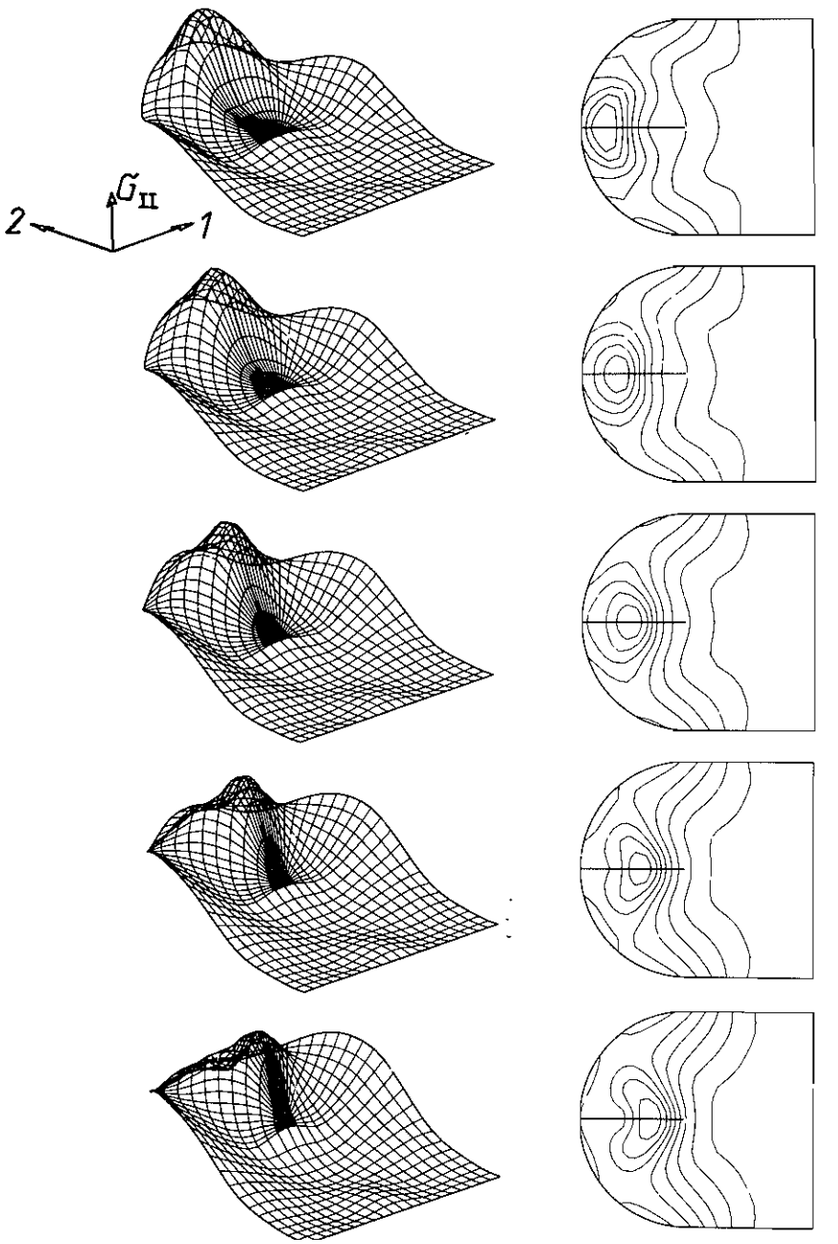

Fig.8b Perspective view and contour lines of principal stress σ_{II} for successive time steps

REFERENCES

1 W.Arrenbrecht and J.Ballmann, in P.L.Butzer and F.Fehér (Eds.), E.B.Christoffel, Birkhäuser, Basel, 1981, pp.449-460
2 J.Ballmann, H.J.Raatschen and M.Staat, Fokussierung von Spannungswellen in Scheiben, SFB 27-Jahresberichte, Aachen, 1981/82
3 T.Belytschko and R.Mullen, in J.Miklowitz and J.D.Achenbach (Eds.), Modern Problems in Elastic Wave Propagation, Wiley, New York, 1978, 67-82
4 M.Braun, in U.Nigul and J.Engelbrecht (Eds.), Proceedings of the IUTAM Symposium on Nonlinear Deformation Waves 1982 Tallinn, Springer, Berlin, 1983,pp379-384
5 R.Burridge, Lacunas in Two-Dimensional Wave Propagation, Proc. Camb. Phil. Soc.,63 (1967) 819-825
6 D.S.Butler, The Numerical Solution of Hyperbolic Systems of Partial Differential Equations in Three Independent Variables, Proc.Roy.Soc.London, 255A (1960) 232-252
7 R.J.Clifton, A Difference Method for Plane Problems in Dynamic Elasticity, Quart.Appl.Math. 25 (1967) 97-116
8 R.Courant, K.O.Friedrichs and H.Lewy, Über die partiellen Differenzengleichungen der mathematischen Physik, Math.Ann., 100 (1928/29) 32-74
9 D.W.Haines and W.D.Wilson, Strain-Energy Density Function for Rubber-Like Materials,J.Mech.Phys.Solids,27 (1979), 331-343
10 C.Heinz, Theoretische Gasdynamik, Vorlesungen an der RWTH Aachen, 1974/75
11 A.Henckels and H.Grönig, in M.Pichal (Ed.), Proceedings of the IUTAM Symposium on Optical Methods in Dynamics of Fluids and Solids 1984 Prague, Springer, Berlin, to be published
12 A.Jeffrey and T.Taniuti, Non-Linear Wave Propagation, Academic Press, New York, 1964
13 W.Johnson, Impact Strength of Materials, Arnold, London, 1983
14 W.Johnson and A.G.Mamalis, in K.Kawata and J.Shiori (Eds.), Proceedings of the IUTAM Symposium on High Velocity Deformation of Solids 1977 Tokyo, Springer,Berlin,1978,pp228-246
15 R.Löhner, K.Morgan and O.C.Zienkiewicz, The Solution of Non-Linear Hyperbolic Equation Systems by the Finite Element Method, Int.J.Num.Meth.Fluids, 4 (1984) 1043-1063
16 M.J.P.Musgrave, Crystal Acoustics, Holden-Day, San Francisco, 1970
17 N.Nakagawa, Y.Fujiwara and R.Kawai, Proceedings of the 27th Japan Congress on Materials Research, Kyoto, 1984
18 R.G.Payton, Elastic Wave Propagation in Transversely Isotropic Media, Nijhoff, The Hague, 1983
19 R.G.Payton, Two Dimensional Wave Front Shape Induced in a Homogeneously Strained Elastic Body by a Point Perturbing Body Force, Arch.Rational Mech.Anal.,32 (1969) 311-330 and 35 (1969) 402-408
20 R.Sauer, Anfangswertprobleme bei partiellen Differentialgleichungen, Springer, Berlin, 1958
21 R.Sauer, Differenzenverfahren für hyperbolische Anfangswertprobleme bei mehr als zwei unabhängigen Veränderlichen mit Hilfe von Nebencharakteristiken, Numerische Mathematik, 5 (1963) 55-67
22 C.Truesdell, General and Exact Theory of Waves in Finite Elastic Strain, Arch. Rational Mech. Anal., 8 (1961) 263-296